# Volcanic hazard assessment at the Campi Flegrei caldera

G. MASTROLORENZO, L. PAPPALARDO, C. TROISE, S. ROSSANO, A. PANIZZA, & G. DE NATALE

*Istituto Nazionale di Geofisica e Vulcanologia, Sezione di Napoli Osservatorio Vesuviano, Via Diocleziano, 328, 80024 Naples, Italy (e-mail: mastro@ov.ingv.it)*

**Abstract:** Previous and new results from probabilistic approaches based on available volcanological data from real eruptions of Campi Flegrei, are assembled in a comprehensive assessment of volcanic hazards at the Campi Flegrei caldera, in order to compare the volcanic hazards related to the different types of events. Hazard maps based on a very wide set of numerical simulations, produced using field and laboratory data as input parameters relative to the whole range of fallout and pyroclastic-flow events and their relative occurrence, are presented. The results allow us to quantitatively evaluate and compare the hazard related to pyroclastic fallout and density currents (PDCs) in the Campi Flegrei area and its surroundings, including the city of Naples.

Due to the dominant wind directions, the hazard from fallout mostly affects the area east of the caldera, and the caldera itself, with the level of probability and expected thickness decreasing with distance from the caldera and outside the eastern sectors. The hazard from PDCs decrease roughly radially with distance from the caldera centre and is strongly controlled by the topographic relief, which produces an effective barrier to propagation of PDCs to the east and northeast, areas which include metropolitan Naples. The main result is that the metropolitan area of Naples would be directly exposed to both fallout and PDCs. Moreover, the level of probability for critical tephra accumulation by fallout is relatively high, even for moderate-scale events, while, due to the presence of topographic barriers, the hazard from PDCs is only moderate and mostly associated with the largest events.

Hazard evaluation for explosive volcanoes in densely populated areas is a major goal of research in volcanology. Tephra fallout and pyroclastic density currents coexist in most explosive eruptions, and their relevance and the way that they extend the area affected by volcanic hazards will depend on the eruption style and magnitude as well as environmental conditions (topography, wind pattern). Therefore, hazard evaluation at an active volcano requires the acquisition of as much data as possible relative to past eruptions and their related effects. Nevertheless, due to the high variability of the eruptive phenomena, the volcanological records are not exhaustive enough to be able to define the whole range of possible events for probabilistic evaluation. A more accurate approach requires the exploration of a wider repertoire of possible events which can be reproduced by numerical simulations, in order to produce probabilistic hazard maps.

Campi Flegrei caldera, which has been active since at least *c.* 39 ka ago, produced a total of *c.* 60 highly explosive eruptions, with VEI ranging between 0 and 6. In most cases tephra fallout from sustained column and pyroclastic density currents has been produced. The mechanism of their formation, their intensity and the extension of the affected area, mainly depend on the eruption magnitude. However, volcanological studies (e.g. Mastrolorenzo 1994; Mastrolorenzo *et al.* 2001) and modelling (Rossano *et al.* 1998) have shown that tephra fallout distribution is strongly influenced by seasonal wind changes, while the spreading of pyroclastic density currents is mostly controlled by the topography of the caldera and its surroundings.

Due to the widespread urbanization of the area around the caldera, and particularly of its surroundings, a quantitative evaluation of the hazards related to such phenomena is necessary to better define of the emergency planning.

In this paper, previous and new results of integrated probabilistic and volcanological approaches to numerical simulations of fallout and PDCs events are presented in order to compare the hazards for different types of events.

## Explosive eruptions at Campi Flegri caldera

The Campi Flegrei (CF) is a volcanic field dominated by a Quaternary 12-km-wide caldera depression formed during two high-magnitude eruptions: the 39 ka BP Campanian Ignimbrite (De Vivo *et al.* 2001) and the 14 ka BP Neapolitan Yellow Tuff (Deino *et al.* 2004) (Fig. 1). After

*From*: TROISE, C., DE NATALE, G. & KILBURN, C. R. J. (eds) 2006. *Mechanisms of Activity and Unrest at Large Calderas*. Geological Society, London, Special Publications, **269**, 159–171.
0305-8719/06/$15.00 

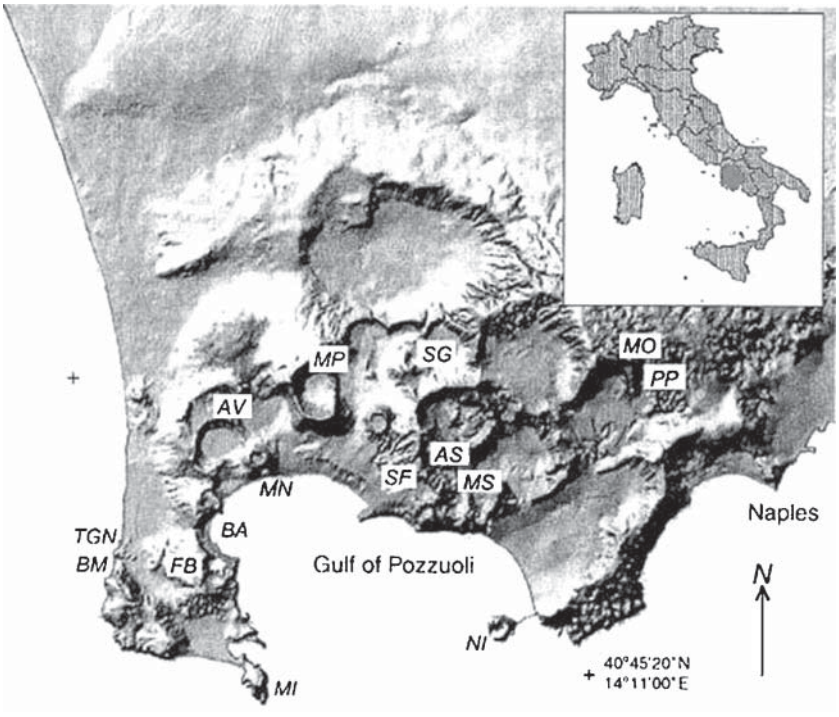


**Fig. 1.** Digital topographic map of the Campi Flegrei Volcanic Field, including monogenetic volcanoes and volcanic formations: AS, Astroni tuff ring; AV, Averno tuff ring; BA, Baia tuff ring; BM, Breccia Museo pyroclastic-flow formation; FB, Fondi di Baia cinder cone; MI, Miseno tuff ring; MN, Monte Nuovo cinder cone; MP, Montagna Spaccata strombolian formation; MS, Monte Spina small-scale pyroclastic flow formation; NI, Nisida tuff cone; SF, Solfatara tuff ring; SG, Senga spatter cone; MO, Minopoli violent strombolian formation; PP, Pomici Principali plinian formation; TGN, Neapolitan Yellow Tuff.

these two main events, *c*. 60 eruptions occurred in the last 14 000 years, from scattered vents located within the caldera.

Explosive eruptions in volcanic history of Campi Flegrei have VEI values of 0 to 5, with erupted masses ranging between less than $10^8$ and $10^{13}$ kg; column height from less than 1 to 45 km, magma eruption rate from hundreds of kg $s^{-1}$ to $10^8$ kg $s^{-1}$; and wide variability in total grain-size distribution, fragmentation and dispersion (Table 1). However, extremely large events are rare, since VEI is generally lower than four. A few very large-scale surge-and-flow deposits are the prevalent eruptive mechanisms in large explosive eruptions, while the tens of intermediate and small-scale deposits occurred as subordinate episodes of more complex eruptive sequences. Effusive activity, with associated lava flows and domes, contributes only a few per cent to the total volume of the volcanic products.

The post-NYT intracalderic activity, prevalently hydromagmatic, mainly formed pyroclastic cones, consisting of interbedded pyroclastic surge and fallout beds. The pure magmatic strombolian, sub-plinian and plinian events, only subordinate, consist of scoria and lapilli beds, with dispersion ranging between a few km$^2$ and some thousands of km$^2$. Small-scale strombolian deposits are mostly dispersed within the caldera rim, while the larger deposits spread outside the caldera in a large area, mostly towards the East.

## Probabilistic approach

Probabilistic hazard maps have been developed for Campi Flegrei for pyroclastic falls and currents, using a generalization of the approaches proposed by Rossano *et al*. (2004) and De Natale *et al*. (2006).

### *Pyroclastic fall*

The transport of tephra in the atmosphere, due to the processes of convection, diffusion and

settling, may be described by the following well-known convection–diffusion–migration equation (Friedlander 2000):

$$\frac{\partial \chi}{\partial t}+\frac{\partial u\chi}{\partial x}+\frac{\partial v\chi}{\partial y}+\frac{\partial w\chi}{\partial z} = \frac{\partial}{\partial x}\left(K_x\frac{\partial \chi}{\partial x}\right)+\frac{\partial}{\partial y}\left(K_y\frac{\partial \chi}{\partial y}\right)+\frac{\partial}{\partial z}\left(K_z\frac{\partial \chi}{\partial z}\right) - \frac{\partial V_{ts}\chi}{\partial x} \quad (1)$$

where $\chi$ is the concentration of tephra (kg m$^{-3}$); $\mathbf{v}\equiv(u,v,w)$ is the wind-velocity vector, $K_x$, $K_y$, $K_z$ are diffusion coefficients; and $V_{ts}$ is the terminal settling velocity. In the hypothesis of low-volume concentration of tephra, $\mathbf{v}$, $K_i$ and $V_{ts}$ depend only on $(x,y,z,t)$ but not on $\chi$, so the equation is linear. Given an expression for such coefficients and suitable boundary and initial conditions, eq. (1) may be solved numerically to give $\chi=\chi(x,y,z,t)$. The mass distribution of tephra after all particles have settled may then be calculated by the integration of vertical fluxes at the surface, at a time much greater than the settling time of the smallest particles in which we are interested. However, such an approach is computationally expensive; in order to calculate the 2D distribution of tephra on the ground for a time larger than the maximum settling time ($t_F$) $t_F > t_s$, we have to compute a 3D field for all times $t < t_F$. According to Suzuki (1983), we can neglect vertical diffusion and convection in the atmosphere with respect to horizontal diffusion and convection, because the former has a much smaller effect than the latter above the atmospheric boundary layer. We have:

$$\frac{\partial \chi}{\partial t}+\frac{\partial u\chi}{\partial x}+\frac{\partial v\chi}{\partial y}=\frac{\partial}{\partial x}\left(K_x\frac{\partial \chi}{\partial x}\right)+\frac{\partial}{\partial y}\left(K_y\frac{\partial \chi}{\partial y}\right) \quad (2)$$

$\chi$ measures of mass of accumulated tephra per unit surface (kg m$^{-2}$). The settling term is implicitly taken into account by considering the solution of eq. (2) at the time corresponding to the fall time of the particles.

Following Bonadonna *et al.* (2005), we use two functional forms for the diffusion coefficient, depending on the fall times (and hence, indirectly, from the sizes) of the particles involved in the diffusion process. The horizontal diffusion of large particles, which is characterized by short fall times, is better described by linear diffusion, in which $K=k$ is constant in time. Diffusion of small particles, on the contrary, is characterized by long fall times, and so is better described by power-law diffusion: $K=Ct^{3/2}$, with $C=0.04$ m$^2$ s$^{-5/2}$. The parameter $K$ is not a turbulent diffusion coefficient but a partly empirical parameter, which takes into account all effects which tend to spread the plume, such as eddy diffusion, gravity flow, and so on. We assume the following initial conditions (IC) and boundary conditions (BC) for equation (2):

$$\begin{aligned} &\text{IC} \quad \chi(x,y,0)=Q\delta(x-x_0,y-y_0) \\ &\text{BC} \quad \lim_{r\longrightarrow\infty}\chi(r,t)=0 \qquad r=\sqrt{x^2+y^2} \end{aligned} \quad (3)$$

corresponding to the instantaneous release at $t=0$ of a mass $Q$ from a vent at coordinates $(x_0,\ y_0)$, in a doubly infinite domain, with the physical constraint that the concentration of tephra decreases at sufficiently large distances from the source. Eq. (2) then yields the analytical solution:

$$\chi=\frac{5Q}{8\pi Ct^{5/2}}\exp\left[\frac{5\left\{(x-ut-x_0)^2+(y-vt-y_0)^2\right\}}{8Ct^{5/2}}\right]$$

for small particles (4)

$$\chi=\frac{Q}{4\pi Kt}\exp\left[\frac{\left\{(x-ut-x_0)^2+(y-vt-y_0)^2\right\}}{4Kt}\right]$$

for large particles (linear diffusivity)

To obtain the distribution of tephra on the ground, we set $t$ equal to the fall time of the particle. The variation of wind speed and direction with altitude, $z$, can be accounted for by dividing the height of the atmosphere into layers of height $\Delta z_i$, each of which is characterized by a constant wind velocity and direction. Particles in the eruption column have different diameters, and arrive at different heights into the column. Particles of grain size $\phi_j$ arriving at height $z_k$ in the column ($z_k \leq H$, the total column height) fall through layers $\Delta z_k=z_k-z_{k-1}, \ldots\ \Delta z_1=z_1-z_0,\ (z_0=0)$. Each layer is crossed in a time $\Delta t_i=\Delta z_i/V_{ts}(z_i\phi_j)$, where the terminal settling velocity $V_{ts}$ depends both on height and on grain size, but not on time, because we can assume that atmospheric density and viscosity at heights of kilometres do not vary with time over the time-scales of tephra deposition. During this time interval, the centre of the Gaussian distribution is displaced by $\Delta x_i=u(z_i)\Delta t_i$ and $\Delta y_i=v(z_i)\Delta t_i$. Hence, when the particles reach the ground, the distribution is:

$$\chi = \frac{5Q}{8\pi C\left(\sum_{i=1}^{K}\Delta t_i\right)^{5/2}} \exp\left[-\frac{5\left\{\left(x - x_0 - \sum_{i=1}^{K}\Delta x_i\right)^2\right\}}{8C\left(\sum_{i=1}^{K}\Delta t_i\right)^{5/2}} - \frac{5\left\{\left(y - y_0 - \sum_{i=1}^{K}\Delta y_i\right)^2\right\}}{8C\left(\sum_{i=1}^{K}\Delta t_i\right)^{5/2}}\right] \text{ for small particles} \quad (5)$$

$$\chi = \frac{Q}{4\pi K\left(\sum_{i=1}^{K}\Delta t_i\right)} \exp\left[-\frac{\left(x - x_0 - \sum_{i=1}^{K}\Delta x_i\right)^2}{4K\left(\sum_{i=1}^{K}\Delta t_i\right)} - \frac{\left(y - y_0 - \sum_{i=1}^{K}\Delta y_i\right)^2}{4K\left(\sum_{i=1}^{K}\Delta t_i\right)}\right]$$

for large particles (linear diffusivity).

The tephra mass is distributed along the height of the column, and has a continuous grain-size distribution. Summing on all heights from 0 to $H$ (column height), and from minimum to maximum diameter, we get the complete grain-size distribution:

$$\chi = \int_0^H \int_{\phi\min}^{\phi_{\max}} f_z(z,\phi) f_\phi(\phi) \frac{5Q}{8\pi C\left[\int_0^z \frac{dz}{V_{ts}(z,\phi)} + t_s\right]^{5/2}} \exp\left[-\frac{5\left\{\left(x - x_0 - \int_0^z \frac{u(z)dz}{V_{ts}(z,\phi)}\right)^2\right\}}{8C\left(\sum_{i=1}^{K}\Delta t_i\right)^{5/2}} - \frac{5\left\{\left(y - y_0 - \int_0^z \frac{v(z)dz}{V_{ts}(z,\phi)}\right)^2\right\}}{8C\left(\sum_{i=1}^{K}\Delta t_i\right)^{5/2}}\right] d\phi dz$$

for small particles, and (6)

$$\chi = \int_0^H \int_{\phi\min}^{\phi_{\max}} f_z(z,\phi) f_\phi(\phi) \frac{Q}{4\pi K\left(\int_0^z \frac{dz}{V_{ts}(z,\phi)} + t_s\right)} \exp\left[-\frac{\left(x - x_0 - \int_0^z \frac{u(z)dz}{V_{ts}(z,\phi)}\right)^2}{4K\left(\sum_{i=1}^{K}\Delta t_i\right)} - \frac{\left(y - y_0 - \int_0^z \frac{v(z)dz}{V_{ts}(z,\phi)}\right)^2}{4K\left(\sum_{i=1}^{K}\Delta t_i\right)}\right] d\phi dz$$

for large particles (linear diffusivity) (where $f_z$ and $f_\phi$ are the distribution functions with respect to height and to diameter, respectively). To the diffusion time, we added the value $t_s$ corresponding to the diffusion of particles inside the eruption column, due to the fact that the eruption column is not really a vertical line, but has a non-zero cross-section.

To calculate $t_s$ we use the semi-empirical expression of Suzuki (1983) for small particles:

$$t_s = \left(\frac{5z^2}{288C}\right)^{2/5}$$

and, for large particles, the expression from Bonadonna *et al.* (2005):

$$t_s = \frac{0.0032z^2}{K}$$

We considered release from an instantaneous point source at time $t=0$ and position $(x_0, y_0)$, while in reality an eruption has a finite duration and spatial extent. To investigate the implication of finite dimensions, we describe a continuous eruption as the integral with respect to time of instantaneous emissions of intensity $I = dQ/dt$. This is possible because of Duhamel's principle for parabolic linear PDEs (such as eq. (1) and eq. (2)). If $f_z$ and $f_\phi$ are independent of time, then all quantities in eq. (6) will be independent of time, with the only possible exception of $I$. Accordingly, we take all parameters except $I$ out of the time integral, and, because the integral of $I$ from 0 to $t$ is equal to $Q$, we have precisely the same result as in the case of an instantaneous eruption. Physically, the reason is that we have already assumed that transport phenomena in

the atmosphere do not depend on initial and final time, but only on the difference between them, and they are also independent of particle concentration. As a result, identical particles released at different times from the same height will remain in the atmosphere for the same time, and fall to the same place.

In order to model a continuous eruption as an instantaneous release, therefore we must assume that $f_z$ and $f_\phi$ do not depend on time, i.e. that the eruption column is a quasi-steady state. This assumption is valid for plinian eruptions after the initial explosion (Woods 1988).

In order to complete the mathematical description of our model, we must specify:

(1) How to compute the terminal settling velocity;
(2) The functional form for grain-size distribution and for vertical mass distribution in the column;
(3) Vertical distribution of wind velocity and directions, with their relative probabilities.

We assume that particles always fall at their terminal settling velocity, i.e. thus neglecting the transient phase of acceleration, which is reasonable, because of the thickness of the vertical layers into which we divide the atmosphere. The expression for the terminal settling velocity of a particle is a critical point; when the velocity of the particle is equal to $V_{ts}$, drag forces due to the air and to the weight of the particle must be balanced:

$$m_p g = \frac{1}{2}\rho_a A C_D V_{ts}^2 \tag{7}$$

where $m_p$ is particle mass, $g$ is gravitational acceleration, $\rho_a$ is air density, $A$ is particle cross-section and $C_D$ is a non-dimensional parameter called the drag coefficient, defined as the ratio between the aerodynamic drag force on the particle and the product of dynamic pressure $1/2\rho_a V$ for the cross-section $A$. $C_D$ depends on the Reynolds number $Re$, defined as:

$$Re = \rho_a V d / \mu \tag{8}$$

where $V$ is the particle velocity relative to the air; $d$ is the particle diameter (mean of the three principal axes for aspherical particles); *and* $\mu$ is air viscosity. If $Re \ll 1$, we are in Stokes' regime, where, for spherical particles, $C_D = 24/Re$, so that we get the following analytical expression for $V_{ts}$:

$$V_{ts} = \frac{\rho_p d^2 g}{18\mu} \tag{9}$$

Outside Stokes' regime ($Re \ll 1$), no analytical solution for $V_{ts}$ has been found up to now, even for simple shapes like spheres. This is due to the non-linearity of the Navier–Stokes equations: partial differential equations governing the viscous flow of Newtonian fluids like air. Experimental expressions are thus needed, but different sets of experimental results for volcanic particles are often in disagreement. Suzuki (1983) found an expression which is a good fit to the various experimental data:

$$\begin{aligned} V_{ts} &= \frac{\rho_p g d^2}{9\mu F^{-0.32}} \rightarrow \\ &\leftarrow + \frac{\rho_p g d^2}{\sqrt{81\mu^2 F^{-0.64} + 1.5\rho_a \rho_p g d^3 \sqrt{1.07 - F}}} \\ d &= \frac{a+b+c}{3} \\ F &= \frac{b+c}{2a} \end{aligned} \tag{10}$$

where $\rho_p$ is particle density; $\rho_a$ is air density; *a, b, c* are the three principal axes with $a$ being the longest one; $\mu$ is air viscosity; $F$ is called the shape factor and is equal to 1 for spherical particles; and $d$ is the mean diameter.

Such an expression works well for low to moderate Reynolds numbers: its limit for $Re \rightarrow 0$ and $F = 1$ is eq. (9), correctly. However, it fails for higher values, because it predicts a decreasing $C_D$, while experimental evidence for volcanic particles shows that the drag coefficient approaches the value of 1 for high $Re$. We thus chose to compute the Reynolds number $Re_L$ which, according to Suzuki's expression, corresponds to a drag coefficient of 1, and use Suzuki's expression for $Re \leq Re_L$, while if $Re > Re_L$, we set $C_D = 1$ and obtain $V_{ts}$ from equation (7). We write $V_{ts}$ for a spherical particle, in order to show that $V_{ts}$ increases with the diameter and the density of the particles:

$$V_{ts} = \sqrt{\frac{4\rho_p d g}{3\rho_a}} \tag{11}$$

Air density and viscosity in the atmosphere depend on height; thus, particles will fall quickly through the higher atmospheric layers, but will slow down at lower heights. The phenomenon is less important for the smallest particles which move in the Stokes' regime; their terminal settling velocity does not depend on density. We will model the dependence of atmospheric

thermodynamic properties according to the US Standard Atmosphere 1976 (Anon. 1976).

We assume that the grain-size distribution is log-normal, e.g. the distribution in ϕ units is normal ($\phi = -\log_2(d)$ where $d$ is the particle diameter in millimetres):

$$f\phi(\phi) = \frac{1}{\sqrt{2\pi}\sigma_d}\exp\left\{-\frac{(\phi-\mu_d)^2}{2\sigma_d^2}\right\} \qquad (12)$$

where $\mu_d$ and $\sigma_d$ are, respectively, mean and standard deviation.

The vertical mass distribution in the column is taken from Connor *et al.* (2001):

$$f_z(z) = \begin{cases} \dfrac{\beta W_0 Y(z)\exp\{-Y(z)\}}{V_{ts}(0,\phi)H\left(1-\left[1+Y(0)\exp\{-Y(0)\}\right]\right)} \\ 0 \end{cases} \qquad (13)$$

$0 \le z \le H$

otherwise

$$Y(z) = \frac{\beta W(z)}{V_{ts}(0,\phi)}$$

$$W(z) = W_0\left(1-\frac{z}{H}\right)^{\lambda},$$

where $W(z)$ is gas velocity at height $z$ and $W_0$ is gas velocity at the vent. In this work it is always assumed that $\lambda = 1$ (Connor *et al.* 2001), since, according to Carey & Sparks (1986), linear variation of $W$ with $z$ is a satisfactory approximation for the major part of the column, except near the top and the bottom. From eq. (13) it may be easily proved that the integral of $f_z$ over $[0,H]$ is 1, and that $f_z \ge 0$ for any $z$, so it is indeed a distribution.

$H$ is a normalization factor which does not change the shape of the function, so there are apparently three parameters $\beta, W_0, V_{ts}(0, f) = V_0$, in eq. (13). However, $f_z$ depends only on the product $Y(0) = \dfrac{\beta W(0)}{V_0} = \dfrac{\beta W_0}{V_0} = Y_0$, so it is a one-parameter distribution. In practice, $W_0$ and $V_0$ are constrained by the physics of the problem, so we study the dependence of $f_z$ on β only. Omitting the simple but tedious calculation, we say that $f_z$ has a maximum in $[0,H]$ if and only if $\beta^3 = V_0/W_0$. The terminal settling velocity at sea-level of big particles is of the order of tens of metres per second, while the eruption velocity is of the order of hundreds of metres per second, so this condition is usually satisfied for all particles when $\beta^3 = 0.1$. The maximum is attained for $z_M = H\left(1-\dfrac{V_0}{\beta W_0}\right)$ and has the value

$$f_z(z_M) = \frac{\beta W_0/V_0}{\varepsilon}\frac{1}{H\left(1-\left(1+\dfrac{\beta W_0}{V_0}\right)\exp\left(-\dfrac{\beta W_0}{V_0}\right)\right)}.$$

So we note that as $\beta \to \infty$, $z_M \to H$, $f_z(z_M) \to \infty$: since the integral of $f_z$ must be 1, this means that larger values of β correspond to more mass being accumulated near the top of the column, and less at lower heights.

In order to handle the wind-velocity term in eq. (1), we adopted the 1953–2000 database of wind velocity and directions measured between 0 and 34 km of elevation from the ground at Brindisi (southern Italy) meteorological station. Average values of wind velocities and frequency of occurrence of wind direction have been computed, from the database, in sectors of 10° and for 10 selected heights. Thus, probabilities can be assigned, at each elevation, to each direction in steps of 10°, and the corresponding wind velocity can be assigned. As previously evidenced by Cornell *et al.* (1983), the average wind directions in the troposphere and stratosphere are almost independent of the height, above 5 km with a nearly westerly prevailing direction in all seasons; in summer, however, there is a higher variability with, above 20 km, a nearly easterly prevailing direction. Figure 2 shows histograms of fallout deposits' dispersal axes relative to several tens of past eruptions from Neapolitan volcanoes (Vesuvius, Campi Flegrei and Ischia). It is evident that there is a good correlation of observed dispersal axes in past eruptions with the relative

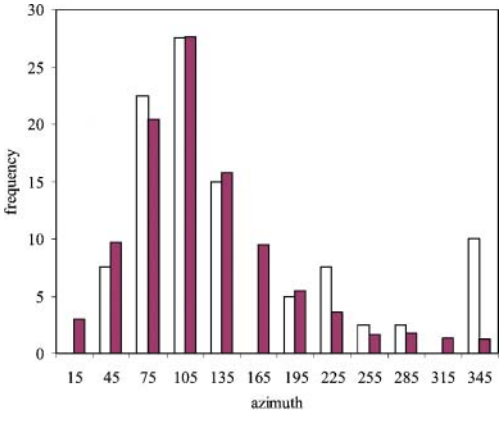


**Fig. 2**. Comparison between the frequency of wind directions collected at Brindisi (Southern Italy) meteorological station in the period 1953–2000 (red) and the observed tephra dispersions of Campanian eruptions in the last 100 ka (white).

frequencies of wind directions as inferred from meteorological data.

*Pyroclastic density currents*

Simulation of pyroclastic density currents (PDCs) was carried out by Rossano *et al.* (2004), by direct and inverse numerical simulation of pyroclastic flows, based on a simple model of a gravity-driven pyroclastic current which stops for *en masse* freezing (Rossano *et al.* 1996, 1998, 2004). The flow is assumed to be incompressible, with a Newtonian or Bingham rheology. Emission from the vent is considered as being steady state from the initiation of eruption.

The physical model of PDCs is described by the equations of uniform flow for a Bingham or Newtonian fluid (McEwen & Malin 1989; Rossano *et al.* 1996). The steady, uniform velocity profile for a Bingham flow in infinitely wide channels is given by:

$$v(z) = \frac{1}{\eta}\left[\frac{\rho g \sin\theta\left(D^2 - z^2\right)}{2} - k\left(D - z\right)\right], \quad (14)$$

where $z \geq D_c$ is the height (measured from the bottom of the channel), $k$ is yield strength, $\rho$ is the density of flow material, $g$ is acceleration due to of gravity, $\theta$ is the slope of ground, $\eta$ is the viscosity, $D$ the total flow depth, and $D_c$ is the plug thickness,

$$D_c = \frac{2\left(kD + \eta v\right) - \sqrt{\left(2kD + 2\eta v\right)^2 - 4k^2D^2}}{2k}. \quad (15)$$

The acceleration of the plug in a wide channel is (McEwen & Malin 1989):

$$\frac{dv_p}{dt} = |a| - \frac{2k}{\rho\left(D + D_c\right)} - \frac{2\eta v_p}{\rho\left(D^2 + D_c^2\right)}, \quad (16)$$

where $v_p$ is plug velocity and $|a|$ is the modulus of the gravity contribution to the flow motion. Resistance terms in the equation describing a Bingham flow unit depend on several factors. For a Bingham flow, the transition from laminar to turbulent flow depends upon two dimensionless numbers, the Reynolds number $Re = \rho v D/\eta$, and the Bingham number $Bi = kD/\eta v$. From empirical relations, Middleton & Southard (1978) observed that, when $Bi$ exceeds about 1.0, the onset of turbulence occurs for $Re/Bi \geq 1000$. According to McEwen & Malin (1989), the frontal air drag is assumed to be negligible, so that the deceleration due to air drag on the upper surface (Perla 1980) of the flow is:

$$\frac{dv}{dt} = -c_a\left(\frac{\rho_a}{\rho}\right)\frac{v^2}{2D} \quad (17)$$

where the constant $c_a$ ranges ranges between 0.1 and 1 (Perla 1980). The matrix of the input parameters for the generation of the PDCs model set includes: vent coordinates; initial velocity and direction of the flow; flow density, thickness and rheological parameters (viscosity and yield strength).

Flow trajectories were computed for a digital topographic model of Campi Flegrei, approximating PDCs to idealized, one-dimensional, mass-independent flows. The kinematics of the material point are governed by the equations given above, with the known values of the local component of acceleration, and the assumed physical properties of the moving flow (initial velocity, density and rheology) and air friction. A large family of flow lines simulates the travel paths of a linear front departing from the vent.

As discussed by Rossano *et al.* (1998), even if we neglect lateral expansion; interaction between distinctive streamlines; and the effects of entrainment and sedimentation, the high density of 1D flow-lines approximates a 2D model. This is particularly true for the high ratio between average PDC thickness and small-scale average landforms of the area.

A large number of individual 2D pyroclastic density currents (PDCs) were simulated spanning a wide range of properties and vent conditions. Each 2D flow, characterized by specific physical properties, is defined by a family of 1D flow-lines that move over a digital elevation model as a gravity-driven current. The whole set of flow models is obtained by sampling a multidimensional matrix of vent position, initial velocity and rheological parameters which control the pyroclastic flow movement.

Equations (14) to (17) have been used to simulate the flows. These show that the parameters which characterize individual pyroclastic currents are: initial velocity, viscosity, density, thickness and yield strength.

Typical values for each parameter have been estimated using the eruption catalogue and field data. The results are summarized in Table 2, which shows the probability of a particular value occurring. All the combinations of the given parameter values are considered in the simulation, each one taken with the cumulative probability given by the product of probabilities of the single parameters. With these choices, hazard maps are computed by extracting, from the whole set of 2800 simulated eruptions, the probabilities of the flow crossing each given area of 1 km$^2$ on the topographic map. The crossing

**Table 1.** *Matrix of input parameters and their relative probability for fallout simulations*

| | **VEI 0** | **VEI 1** | **VEI 2** | **VEI 3** | **VEI 4** | **VEI 5** |
|---|---|---|---|---|---|---|
| Probability | 0.01 | 0.09 | 0.2 | 0.4 | 0.2 | 0.09 |
| Column height (km) | 0.01–0.1 | 0.1–1 | 1–5 | 3–15 | 10–25 | 25–35 |
| Erupted mass (kg) | $10^6$–$10^7$ | $10^7$–$10^9$ | $10^9$–$10^{10}$ | $10^{10}$–$10^{11}$ | $10^{11}$–$10^{12}$ | $10^{12}$–$10^{13}$ |
| Initial velocity (m $s^{-1}$) | 10–100 | 10–200 | 100–200–400 | 200–400–600 | 200–400–600 | 200–400–600 |
| *Md*ϕ (probability) | –4,–3,–1 (0.25,0.5,0.25) | –4,–3,–1 (0.25,0.5,0.25) | –3,–2,–1 (0.25,0.5,0.25) | –2,–1,0 (0.2,0.4,0.4) | –2,–1,0 (0.2,0.4,0.4) | –2,–1,0 (0.2,0.4,0.4) |
| *Md*ϕ min | 7 | 7 | 7 | 7 | 7 | 7 |
| *Md*ϕ max | –7 | –7 | –7 | –7 | –7 | –7 |
| σϕ | 1, 0.5 | 1, 0.5 | 1, 0.5 | 1, 0.5 | 1, 0.5 | 1, 0.5 |
| β | 0.008–0.2 | 0.008–0.2 | 0.008–0.2 | 0.008–0.2 | 0.008–0.2 | 0.1–0.6 |
| *k* | 2000–3000 | 2000–3000 | 2000–3000 | 2000–3000 | 2000–3000 | 2000–3000 |

**Table 2.** *Matrix of input parameters and their relative probability for PDC simulations (Rossano* et al. *2004)*

| | | | | | |
|---|---|---|---|---|---|
| Initial velocity (m/s) | 2 (*0.1*) | 35 (*0.3*) | 65 (*0.3*) | 100 (*0.2*) | 150 (*0.1*) |
| Flow thickness (m) | 0.5 (*0.1*) | 3 (*0.3*) | 6 (*0.3*) | 10 (*0.2*) | 20 (*0.1*) |
| Viscosity (Pa s) | 1 (*0.2*) | 10 (*0.3*) | 100 (*0.3*) | 500 (*0.2*) | |
| Yield Strength | 0 (*0.5*) | 10 (*0.2*) | 100 (*0.2*) | 1000 (*0.1*) | |
| Density (kg $m^{-3}$) | 10 (*0.5*) | 100 (*0.4*) | 1000 (*0.1*) | | |

probabilities are computed as the sum of probabilities from each given eruption for which at least one flow crosses the area.

## Hazard maps

Hazard map computation was achieved using a probabilistic approach to simulate a large, mostly complete set of eruptions, whose relative distribution in energy classes (VEI) matches the one observed in the intrinsically incomplete set of past eruptions. The incompleteness of the historical record derives from two main sources: the first is the scarce sampling of the eruption spectrum, which, however, does give us the general statistical distribution of eruptions in each class of VEI; the second is the scarce spatial sampling of eruptive vents, from which we can still infer some information about its statistical distribution.

Both fallout and PDCs have been simulated by discrete sampling of a multidimensional matrix of input parameters (Tables 1 & 2), based on field evidence and inferences as well as data reported in the literature and corresponding to the whole range of volcanic explosivity index (VEI) that occurred in the history of Campi Flegrei.

For fallout hazard assessment, three different scenarios have been considered, corresponding to distinctive sampling of the whole matrix of input parameters: (1) an upper-limit scenario relative to the worst-case event (VEI 5); this is useful to determine the upper-limit value of tephra-fall accumulation; (2) an eruption range scenario (VEI 1–4) which excludes the upper-limit high-risk but very-rare events, as well as the lowest VEI events that are frequent but have very low risk; this represents the most probable scenario expected for medium–short term; (3) a whole-range eruption scenario (VEI 0–5), which includes all the possible VEI events (long-lasting activity scenario). For the three scenarios, hazard maps relative to the critical load for the roof collapse of 200 kg $m^{-2}$ have been drawn (Fig. 3).

In addition, the absolute probability (conditional probability) that the critical load will be exceeded in the case of eruption, has been also computed for the whole eruption scenario (Fig. 4).

For PDCs hazard map, due to the mass-independent nature of the flow model, a single whole-range scenario was considered by Rossano *et al.* (2004), (Fig. 5). It includes all possible combinations of flow parameters which

**Fig. 3.** Yearly probability hazard maps computed for the minimum load for the roof collapse of 200 kg $m^{-2}$ run for (**a**) upper limit scenario (VEI 5); (**b**) eruption-range scenario (VEI 1–4); (**c**) whole-range eruption scenario (VEI 0–5).

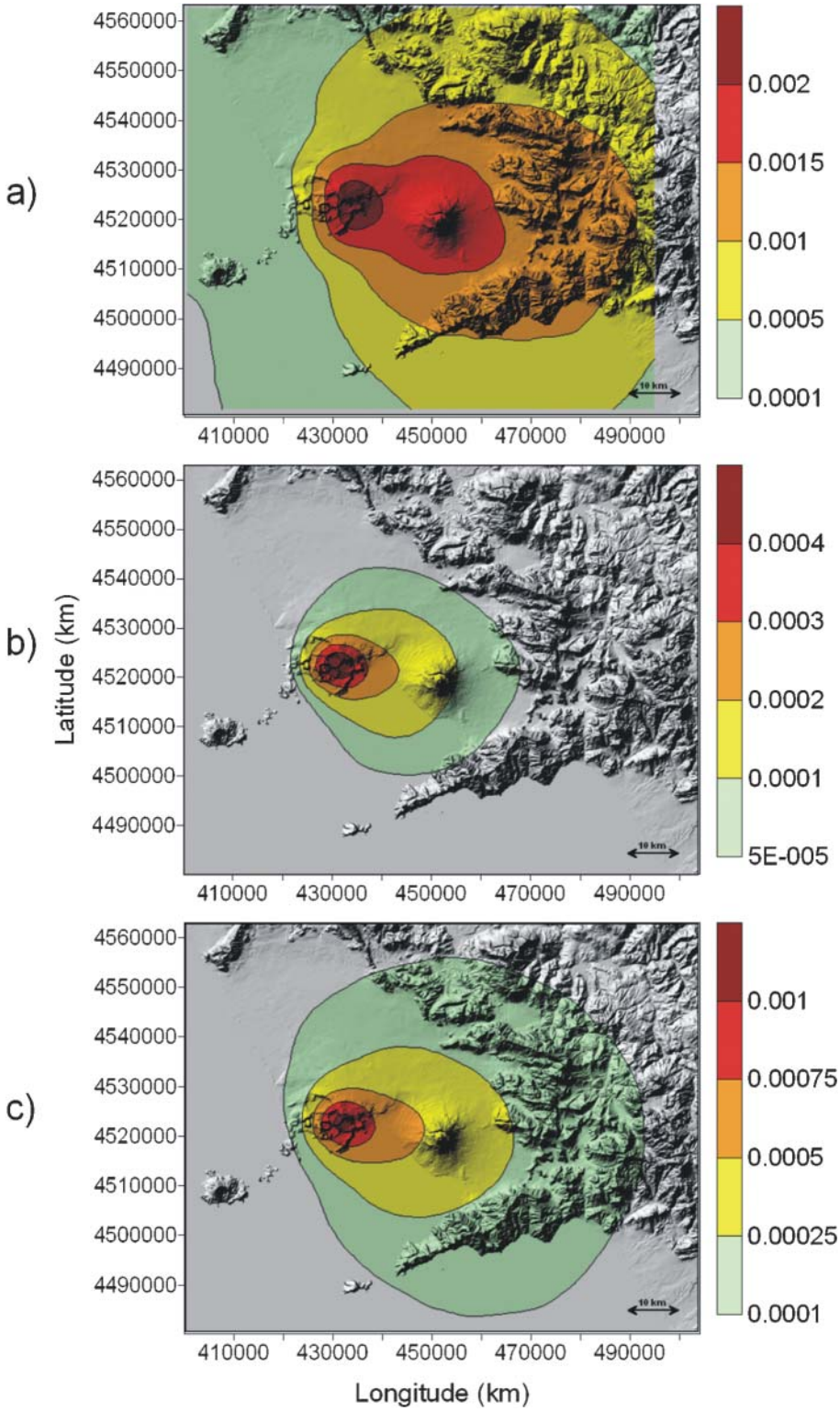
a)
b)
c)
Latitude (km)
Longitude (km)
4560000
4550000
4540000
4530000
4520000
4510000
4500000
4490000
410000
430000
450000
470000
490000
10 km
0.002
0.0015
0.001
0.0005
0.0001
0.0004
0.0003
0.0002
0.0001
5E-005
0.001
0.00075
0.0005
0.00025
0.0001

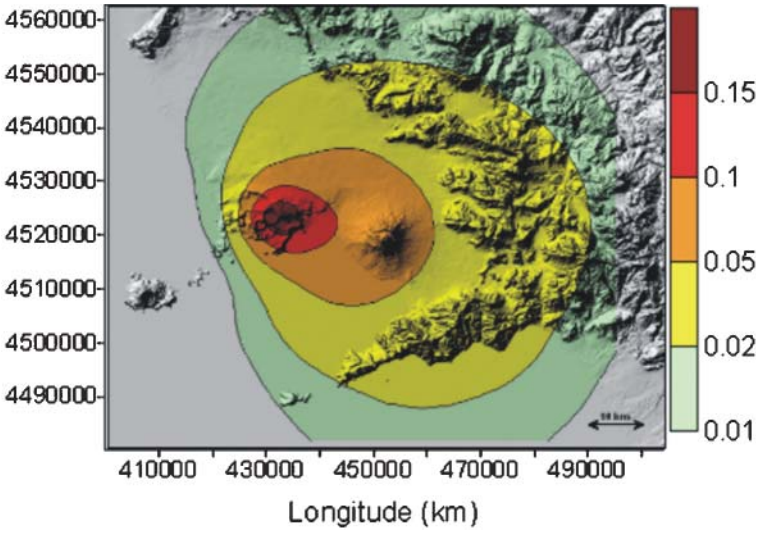


**Fig. 4.** Conditional probability hazard maps relative to the minimum load for the roof collapse of 200 kg $m^{-2}$ run whole-range eruption scenario (VEI 0–5).

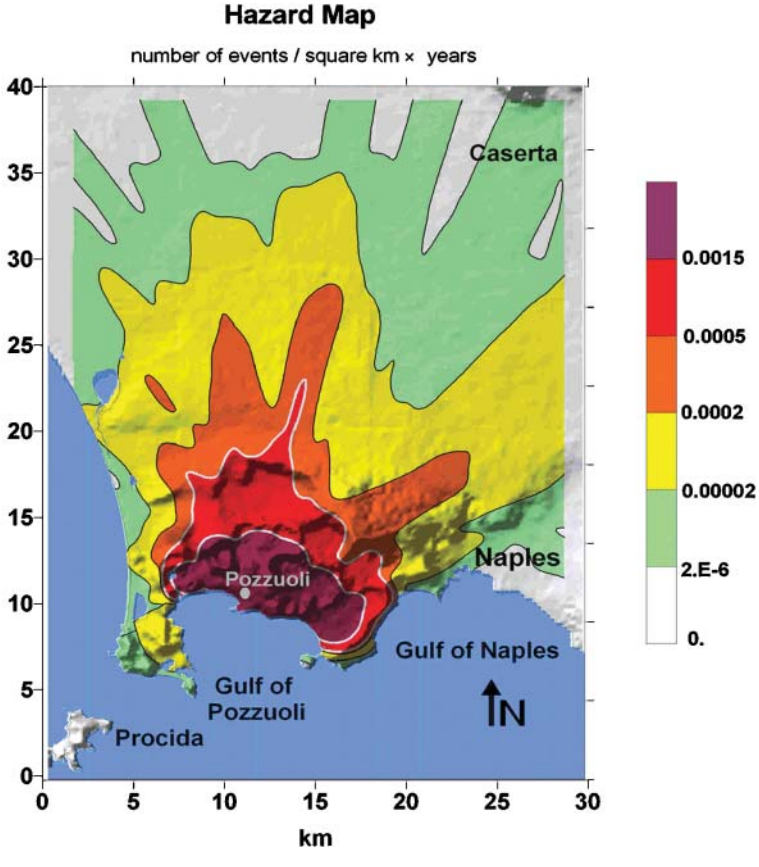


**Fig. 5.** Yearly probability hazard map for PDCs computed for whole-range scenario (VEI 0–5).

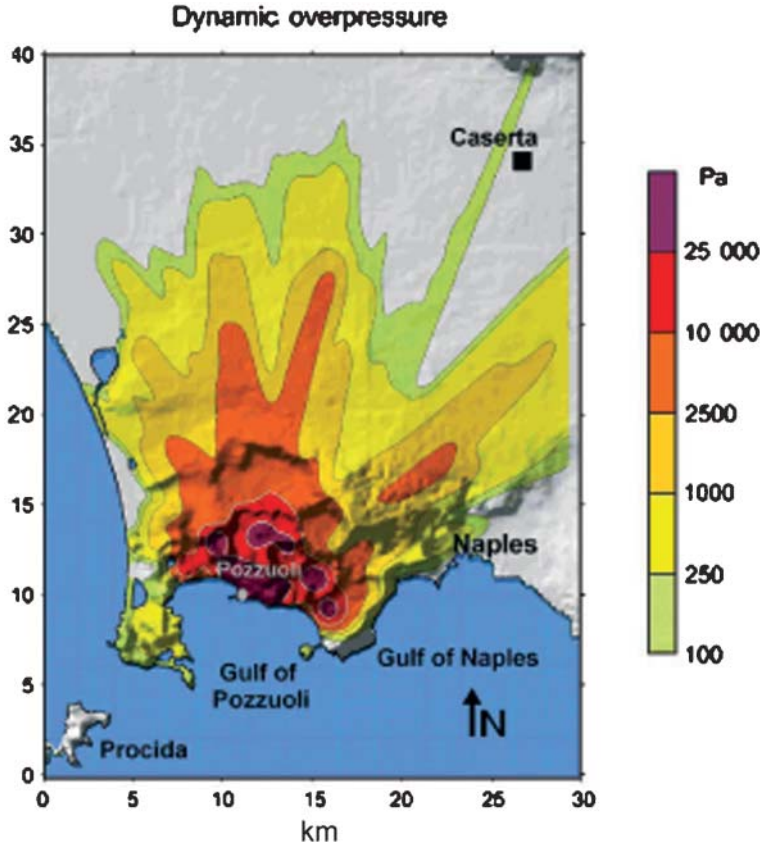


**Fig. 6.** Dynamic overpressure for PDCs.

can characterize both small- and large-scale events. In fact, according to the volcanic history of Campi Flegrei, even eruptions of a moderate magnitude could generate high-mobility PDCs. Dynamic overpressure maps computed by Rossano *et al.* (2004) are also presented in Figure 6.

## Discussion and conclusions

Probabilistic volcanological approaches provide the first complete, statistically accurate description of the expected tephra fallout and PDCs hazard from the whole variety of possible explosive events at Campi Flegrei, in the Neapolitan area and its surroundings.

For fallout events, in the case of small and intermediate eruptions (VEI not exceeding 3) with a relatively low eruptive column, highly variable low tropospheric winds prevail, causing the tephra to be potentially dispersed in all directions with near-homogeneous probability. However, in these cases, critical tephra load and the associated hazards are confined to within few km of the vents inside the caldera boundary.

Outside the caldera, the hazard level of depends strictly on the scenario being considered. In the case of the eruption range scenario, which is the most useful for civil-defence, significant (0.00025 events/year) hazards for critical tephra load characterize a wide sector northeast to southeast within a range of about 10 km from the caldera centre, which includes the western part of Naples. The area north of Campi Flegrei is exposed to a moderate hazard level. The sectors west and south of caldera, exposed to a low hazard level, are also less important in terms of risk, being mostly occupied by the sea. In the whole range and upper-limit scenarios, an area up to 60 km from the caldera is potentially exposed to a critical load. In the whole range scenario, the yearly hazard for the area northeast to southeast of the caldera, between *c.* 10 and 60 km, ranges respectively between about

0.0005 events/year to 0.0001 events/year potentially affecting the districts of Naples, Caserta, Avellino and Salerno. For the upper-limit scenario, the yearly probability for critical-loading hazard maps is $^{3}$0.0015 events/a within 30 km of the vent, and a decrease up to $^{3}$0.001 events/a at a distance of 60 km. In addition, the absolute probability (conditional probability) that the critical load will be exceeded in the case of an eruption has been also computed for the whole eruption scenario. Figure 6 shows that a significant probability level of 10% affects the area within 30 km of the caldera.

The numerical simulation of millions of pyroclastic flow-lines, for a wide range of reasonable rheological properties over a topographic model of Campi Flegrei, reveals that:

(1) The maximum range of the most mobile flows is *c.* 20 km. Such flows are mostly Newtonian, and are very fast ($v_0 > 100$ m s$^{-1}$), with $a > 0$ m moving front, which spreads in a circular pattern. They pass over up to 400-m-high topographic barriers with only moderate effects. However, these flows are rare in the recent history of Campi Flegrei.
(2) Most of the flows with intermediate mobility suffer the effects of the main topographic barriers, and in particular of the western steep slope of Posillipo Hill (*c.* 200 m a.s.l.). They pass through the valleys contouring the crater rims and generate an irregular areal pattern of distribution. Most of the moderate- and small-scale pyroclastic flows do not affect the city of Naples.
(3) Very viscous, slow-moving flows are strongly controlled by the rugged topography of the volcanic field. They are mostly confined within a few km of the vent in small valleys and even within older crater relicts.
(4) Very high hazard levels and high dynamic overpressure mostly affect the inner caldera area; however, the eastern part of the plain north of Campi Flegrei, and even Naples, are exposed to the effects of PDCs, but with a probability one order of magnitude less than that calculated for Campi Flegrei.

Comparison of the pyroclastic fall and flow-hazard maps reveals the following evidence. Within the caldera rim, the hazard from fallout and PDCs is nearly equivalent (higher than 0.0002 events/year), while outside the caldera within a range of *c.* 20 km, which includes the provinces of Naples and Caserta, the PDC hazard and dynamic overpressure drop to values more than one order of magnitude less than the corresponding hazard for critical tephra load. The area of Naples outside the caldera rim is exposed to a relatively low level of PDC hazard (2E-6 events/year), but lies within the zone of significant fallout hazard (0.0005 events/year).

## References


Anon. 1976. *US Standard Atmosphere 1976*. US Government Printing Office, Washington, DC.

Bonadonna, C., Connor, C. B., Houghton, B. F., Connor, L., Byrne, M., Laing, A. & Hincks, T. K. 2005. Probabilistic modeling tephra dispersal: hazard assessment of a multiphase rhyolitic eruption at Tarawera, New Zealand. *Journal of Geophyical Research*, **110**(B03203), doi:10.1029/2003JB002896.

Carey, S. & Sparks, R. S. J. 1986. Quantitative models of the fallout and dispersal of tephra from volcanic eruption columns. *Bulletin of Volcanology*, **48**, 109–125.

Cornell, W., Carey, S. & Sigurdsson, H. 1983. Computer simulation of transport and deposition of the Campanian Y-5 ash. *Journal of Volcanology and Geothermal and Research*, **17**, 89–109.

Connor, B. C., Hill, E. B., Winfrey, B., Franklin, M. N. & La Femina, C. P. 2001. Estimation of volcanic hazards from tephra fallout. *Natural Hazards Review*, **February**, 33–42.

Deino, A. L., Orsi, G., de Vita, S. & Piochi, M. 2004. The age of the Neapolitan Yellow Tuff caldera-forming eruption (Campi Flegrei caldera – Italy) assessed by $^{40}$Ar/$^{39}$Ar dating method. *Journal of Volcanology and Geothermal Research*, **133**, 157–170.

De Natale, G., Troise, C., Pingue, F., Mastrolorenzo, G. & Pappalardo, L. 2006. The Somma – Vesuvius volcano (Southern Italy) Structure, dynamics and hazard evolution. *Earth-Science Reviews*, **74**, 73–111.

De Vivo, B., Rolandi, G. *et al.* 2001. New constraints on the pyroclastic eruptive history of the Campanian Volcanic Plain (Italy). *Mineralogy and Petrology*, **73**, 47–65

Frielander, S. K. 2000. *Smoke, Dust and Haze: Fundamentals of Aerosol Behaviour*. John Wiley, New York.

McEwen, A. S. & Malin, M. C. 1989. Dynamics of Mount St. Helens' 1980 pyroclastic flows, rockslide-avalanche, lahars, and blast. *Journal Volcanology and Geothermal Research*, **37**, 205–231

Mastrolorenzo, G. 1994. Averno tuff ring in Campi Flegrei (south Italy). *Bulletin of Volcanology*, **56**, 561–572.

Mastrolorenzo, G., Brachi, L. & Canzanella, A. 2001. Vesicularity of various types of pyroclastic deposits of Campi Flegrei volcanic field: evidence of analogies in magma rise and vesiculation machanisms. *Journal of Volcanology and Geothermal Research*, **109**, 41–53.

Middleton, G. V. & Southard, J. B. 1978. *Mechanism of Sediment Movement*. SEPM, Eastern Section, Short Course Lecture Notes.

PERLA, R. I. 1980. Avalanche release, motion, and impact. *In*: COLBECK, S. C. (ed.) *Dynamics of Snow and Ice Avalanches*. Academic Press, New York, NY, 397–462.

ROSSANO, S., MASTROLORENZO, G., DE NATALE, G. & PINGUE, F. 1996. Computer simulation of pyroclastic flow movement: an inverse approach. *Geophysical Research Letters*, **23**, 3779–3782.

ROSSANO, S., MASTROLORENZO, G. & DE NATALE, G. 1998. Computer simulations of pyroclastic flows on Somma–Vesuvius volcano, *Journal of Volcanology and Geothermal Research*, **82**, 113–137.

ROSSANO, S., MASTROLORENZO, G. & DE NATALE, G. 2004. Numerical simulation of pyroclastic density currents on Campi Flegrei topography: a tool for statistical hazard estimation. *Journal of Volcanology and Geothermal Research*, **132**, 1–14.

SUZUKI, T. 1983. A theoretical model for dispersion of tephra. *In*: SHIMOZURU, D. & YOKOYAMA, I. (eds) *Arc Volcanism: Physics and Tectonics*, Terra Scientific Publishing Company (Terrapub), Tokyo, 95–113.

WOODS, A. W. 1988. The fluid dynamics and thermodynamics of eruption columns. *Bulletin of Volcanology*, **50**, 169–193.